

FuncGenFoil: Airfoil Generation and Editing Model in Function Space

Jinouwen Zhang^{1*}, Junjie Ren^{1,2}, Aobo Yang³, Yan Lu^{1,4}

Lu Chen^{1,5}, Hairun Xie^{6,7}, Jing Wang^{6,8}

Miao Zhang⁶, Wanli Ouyang^{1,4}, Shixiang Tang^{1,4*}

¹Shanghai Artificial Intelligence Laboratory, ²Fudan University

³Hong Kong University of Science and Technology, ⁴The Chinese University of Hong Kong

⁵State Key Lab of CAD&CG, Zhejiang University, ⁶Shanghai Aircraft Design and Research Institute

⁷Innovation Academy for Microsatellites of CAS, ⁸Shanghai Jiao Tong University

*zhangjinouwen@pjlab.org.cn, *tangshixiang@pjlab.org.cn

Abstract

Aircraft manufacturing is the jewel in the crown of industry, among which generating high-fidelity airfoil geometries with controllable and editable representations remains a fundamental challenge. While existing deep-learning-based methods rely on predefined parametric function families, e.g., Bézier curves and discrete point-based representations, they suffer from inherent trade-offs between expressiveness and resolution flexibility. To tackle this challenge, we introduce **FuncGenFoil**, a novel function-space generative model that directly learns functional airfoil geometries. Our method inherits both the advantages of arbitrary resolution sampling and the smoothness of parametric functions, as well as the strong expressiveness of discrete point-based functions. Empirical evaluations on the AFBench dataset demonstrate that **FuncGenFoil** improves upon state-of-the-art methods in airfoil generation by achieving a relative **-74.4%** label error reduction and **+23.2%** diversity increase on the AF-200K dataset. Our results highlight the advantages of function-space modeling for aerodynamic shape optimization, offering a powerful and flexible framework for high-fidelity airfoil design. Our code will be released.

1 Introduction

The airfoil inverse design problem serves as a central aspect of aircraft manufacturing. Traditionally, given geometric requirements, engineers first select the most similar airfoils from well-known airfoil datasets (e.g., NACA [Cummings *et al.*, 2015]) and leverage the **trial-and-error** strategy [Sharma *et al.*, 2021]. Considering the mission of the aircraft, an initial airfoil design that meets the design conditions is preliminarily created. Then, through rounds of physical analysis, such as aerodynamics and mechanics, the airfoil is iteratively optimized to achieve better performance until the requirements are met. In practice, such direct design procedures are highly inefficient and time-consuming, often taking months. To minimize development and design time, as well as associated

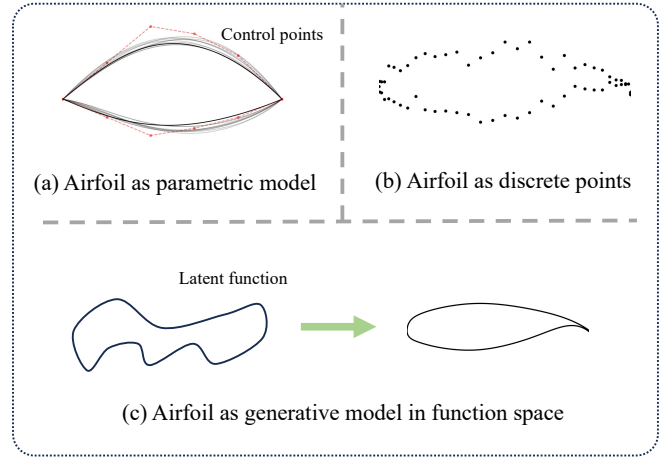


Figure 1: The conceptual difference between FuncGenFoil and previous airfoil representation methods. In many previous approaches, airfoils are represented either as parametric models, as shown in (a), or as discrete point-based models, as shown in (b). In contrast, (c) illustrates FuncGenFoil’s approach, where an airfoil is treated as a continuous function mapped from a latent function, enabling a generative model in function space.

costs, automatic design methods have been introduced as efficient alternatives in aircraft manufacturing engineering. In particular, machine learning-based design and optimization techniques have gained significant attention. However, before applying algorithms to airfoil design, it is crucial to determine appropriate methods for representing airfoils within these algorithms.

Existing methods for airfoil representation can generally be divided into two categories: parametric-model-based approaches [Xie *et al.*, 2024] and discrete-point-based methods [Liu *et al.*, 2024; Sekar *et al.*, 2019]. First, parametric-model-based methods predefine function families, e.g., Bézier curves [Chen and Fuge, 2021], Hicks-Henne curves, and NURBS, and leverage mathematical optimization techniques or generative models to determine the parameters of these functions for a new airfoil. These methods rigorously preserve key geometric properties of the defined functional families, e.g., high-order smoothness. Furthermore,

such functional representations of airfoils allow for arbitrary sampling of control points in real manufacturing, given the constraints of engineering precision. Despite these benefits, parametric-model-based methods suffer from a significantly reduced design space, *i.e.*, selecting a specific function family excludes the possibility of other shapes, which limits the upper bound of airfoil design algorithms. Second, discrete-point-based methods directly generate multiple points to represent airfoil shapes. These methods maximize the design space of airfoils but cannot maintain some important mathematical properties, *e.g.*, continuity. Furthermore, they cannot directly generate control points at arbitrary resolutions because the number of generated points is typically fixed for each model after training.

To address the trade-offs between these two mainstream approaches, we ask: *Can we design an algorithm that leverages the advantages of both?*

In this paper, we answer this question by proposing FuncGenFoil, a novel function-space generative model for airfoil representation (see Fig. 1). Different from previous data-driven and generative methods, *e.g.*, cVAE [Kingma, 2013] and cGAN [Mirza, 2014], which directly generate discrete points, our approach models airfoil geometry using a general continuous function approximator [Anandkumar *et al.*, 2019; Li *et al.*, 2021; Kovachki *et al.*, 2023; Azizzadenesheli *et al.*, 2024], *i.e.*, neural operator architectures. Simultaneously, it leverages recent advances in generative methods, *e.g.*, diffusion models [Ho *et al.*, 2020a] and flow matching models [Lipman *et al.*, 2022], to generate diverse airfoils beyond the design space of any predefined geometry function. Our method has the advantages of both parametric-model-based approaches and discrete-point-based methods. Due to its functional representation, the generated airfoil is continuous and can be sampled at arbitrary resolutions, making it easier to manufacture. Moreover, thanks to the general functional approximator nature of neural operators, our method can explore a broader design space beyond predefined functional families.

Specifically, we leverage the flow matching framework [Lipman *et al.*, 2022], an improved alternative to diffusion models, and FNO [Li *et al.*, 2021], a resolution-free neural operator, as the backbone of our generative model to design FuncGenFoil. In the forward process, we perturb the airfoil into a noise distribution through straight flows. In the backward process, we reconstruct the airfoil by reversing the flow direction. By minimizing the distance between the reconstructed airfoils and actual airfoils, we learn the neural operators that enable us to generate airfoils from functions of Gaussian process. Beyond generation, our method also supports airfoil editing by incorporating the airfoils to be edited as conditions for the generative model.

In summary, our main contributions are threefold: (1) We propose generating airfoil shapes in the functional space to achieve important properties for the aircraft engineering, *i.e.*, arbitrary-resolution control point sampling and maximal design space; (2) We design FuncGenFoil, the first controllable airfoil generative model in the functional space, which effectively incorporates neural operator architectures into the generative model; (3) We further enhance FuncGenFoil with

airfoil editing capabilities through minimal adaptations. Experimental results on the AFBench dataset indicate that our proposed method achieves state-of-the-art airfoil generation quality, reducing label error by 74.4% and increasing diversity by 23.2% on the AF-200K dataset, as validated by aerodynamic simulation analysis. In addition, our method is the first to successfully perform airfoil editing by fixing and dragging at any position, achieving nearly zero MSE error (less than 10^{-7}).

2 Related Works

Generative Models. Generative models based on score matching [Ho *et al.*, 2020b; Song *et al.*, 2021] and flow matching [Lipman *et al.*, 2023; Tong *et al.*, 2024] have significantly advanced machine learning, achieving state-of-the-art results in areas such as image generation [Rombach *et al.*, 2022], text generation [Gat *et al.*, 2024], and video generation [Ho *et al.*, 2022; Polyak *et al.*, 2024]. However, most of these models operate in finite-dimensional spaces and rely on fixed discretizations of data. Such formulations hinder transferability across discretizations and ignore function-level constraints (*e.g.*, continuity, smoothness), motivating the need for function-space generative modeling.

Neural Architecture for Functions space Designing neural architectures to handle function spaces remains a major research challenge. Standard networks typically assume fixed-size inputs, making them unsuitable for arbitrary resolutions. Implicit Neural Representations like SIREN [Sitzmann *et al.*, 2020] harness random Fourier features [Rahimi and Recht, 2007] to represent continuous and differentiable objects through position embeddings. Similarly, NeRF [Mildenhall *et al.*, 2021] treats input coordinates as continuous variables, offering flexible resolution for function outputs. Neural operators [Anandkumar *et al.*, 2019; Li *et al.*, 2021; Kovachki *et al.*, 2023; Azizzadenesheli *et al.*, 2024] and Galerkin transformers [Cao, 2021] further generalize neural architectures to process sets of points as functional inputs, enabling function-space learning.

Generative Models in Function Space. In generative modeling, early Neural Processes [Garnelo *et al.*, 2018b; Garnelo *et al.*, 2018a] drew on Gaussian Processes [Rasmussen, 2003], and later methods such as GASP [Dupont *et al.*, 2022b], Functia [Dupont *et al.*, 2022a], and GANO [Rahman *et al.*, 2022] treat data as function evaluations to enable discretization-independent learning. Energy-based and diffusion models [Lim *et al.*, 2023; Kerrigan *et al.*, 2023; Lim *et al.*, 2025; Pidstrigach *et al.*, 2023; Franzese *et al.*, 2024] along with flow-based approaches like FFM [Kerrigan *et al.*, 2024] and OpFlow [Shi *et al.*, 2024] further extend these ideas. Ultimately, creating comprehensive generative models in function space requires defining suitable stochastic processes, score operators, and consistent neural mappings with specialized training for numerical stability—challenges that remain largely unresolved.

Airfoil Design and Optimization. Airfoil design is critical for aerodynamic performance in systems such as aircraft, race cars, and wind turbines. Geometric parameterization enables efficient modeling and optimization of air-

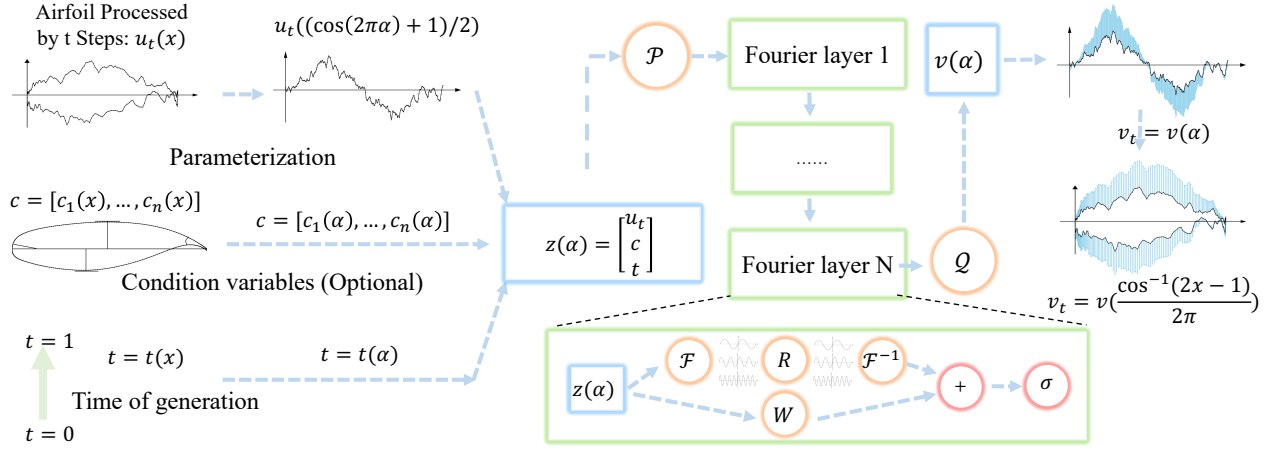


Figure 2: Overview of **FuncGenFoil**'s neural network. The model is a Fourier Neural Operator, but any other neural operator capable of general-purpose function-space approximation may be used. The model takes as input a function u_t (at any resolution d), design condition variables c , and the generation time t . It then processes these as an operator and outputs the current velocity operator $v_\theta(u_t, c, t)$ of the ODE for generation.

foil shapes. Free-Form Deformation (FFD) [Mortenson, 1999], B-splines [Farin, 2002], or NURBS [Schoenberg, 1964]—and is used in CAD/CAE tools like ESP [Dannenhoffer, 2024] and OpenVSP [Hahn, 2010]—but its independent control points can lead to local optima, instability, and high dimensionality. Modal parameterization methods, including Proper Orthogonal Decomposition [Berkooz *et al.*, 1993], global modal [Brüls *et al.*, 2007], and compact modal approaches [Li and Zhang, 2021], address dimensionality by capturing global features with fewer variables, yet their linear reduction struggles with large deformations and detailed edits. In contrast, the Class-Shape Transformation (CST) [Kulfan, 2008] offers intuitive physical interpretation and differentiability but is limited in handling significant deformations and is sensitive to parameter selection. Thus, a high-degree-of-freedom geometric representation is needed to support arbitrary shape modifications while accurately capturing highly nonlinear deformations with stability and robustness.

Recently, with the rise of generative models in the AI field, airfoil design has increasingly adopted generative models such as VAE, GAN and diffusion models [Chen and Fuge, 2021; Li *et al.*, 2022; Xie *et al.*, 2024; Yang *et al.*, 2024; Wei *et al.*, 2024a; Liu *et al.*, 2024], as well as CFD meshes [Wei *et al.*, 2023; Wei *et al.*, 2024b], to enhance the representation of airfoil shapes in a generative manner. These models establish an effective transformation from a latent space to the airfoil space. Previous works have primarily focused on modeling the discrete points of airfoils, which limits their flexibility for downstream tasks.

3 FuncGenFoil: Function-space Generative Model for Airfoils

Different from existing airfoil generation methods, FuncGenFoil is constructed as a function-space generative model, capable of producing airfoil geometries as continuous functions instead of discrete points, leveraging the advantages of

both parametric-model-based and discrete-point-based methods. We detail the process for airfoil generation and editing tasks, respectively.

3.1 Airfoil Generation

The entire FuncGenFoil is essentially an ordinary differential equation (ODE) generative model that generates airfoil by solving an ODE continuous time $t \in [0, 1]$ as follows:

$$du_t = v_t dt, \quad (1)$$

where v_t is a velocity that gradually transforms an assumed latent coding u_0 (u_t at $t = 0$) sampled from stochastic process \mathcal{P} into an airfoil function u_1 belonging to the target airfoil distribution \mathcal{Q} .

Velocity Operator. Obviously, the velocity v_t is the key, we achieve it by establishing a parameterized velocity operator $v_\theta(u_t, c, t)$ with model weights θ , *i.e.*, $v_t = v_\theta(u_t, c, t)$. To enable the velocity operator v_θ an ability to take the airfoil shape function as input, we build v_θ as a function-space generative model by Operator Flow Matching [Shi *et al.*, 2025] as shown in Fig. 2. Specifically, v_θ consists of stacked multiple Fourier Neural Operator layers and it takes noised airfoil u_t (at any resolution d), condition variables (optional) and a timestamp t as inputs, deriving v_t .

Airfoil Geometry Parametrization. Since an airfoil has circular topology, we introduce the variable $\alpha \sim [0, 2\pi]$ for convenience. We denote $y(\alpha) = u_1(\alpha)$ and $x(\alpha) = \frac{\cos(2\pi\alpha)+1}{2}$, achieving the function of airfoil $u_0 = (x(\alpha), y(\alpha))$.

Training. We train v_θ under the denoising training process. Given an airfoil geometry u_1 , we compute its corresponding noised sample at time t as follows:

$$u_t = t \times u_1 + (1 - t) \times u_0 \quad (2)$$

¹For the remainder of this paper, we omit the explicit dependence on α for clarity.

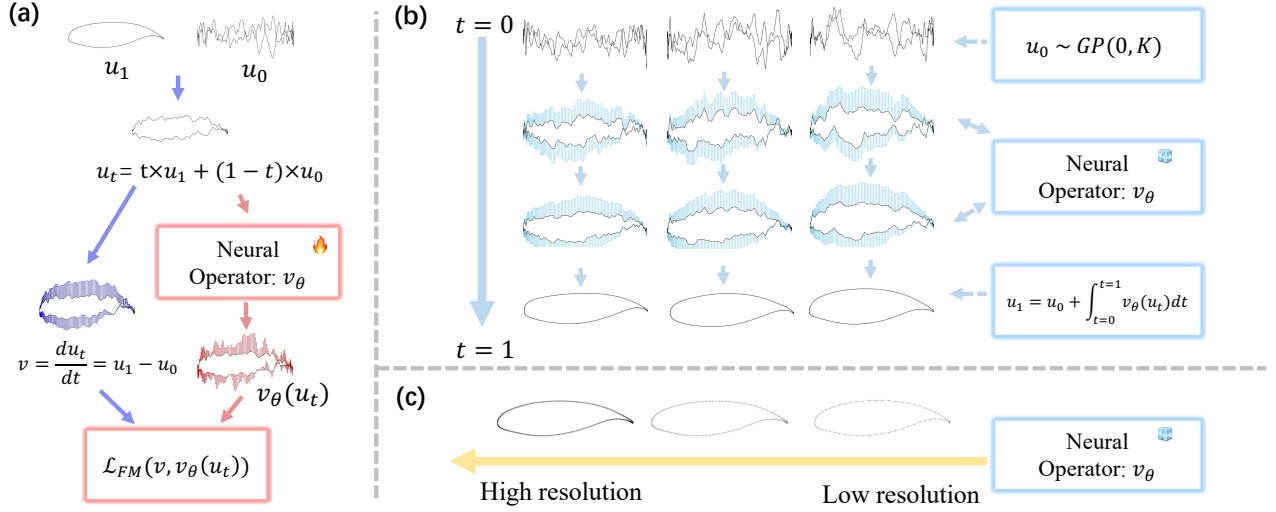


Figure 3: Airfoil generation by **FuncGenFoil**. We first sample latent function from a zero-mean Gaussian process with kernel function K at any resolution. Then we solve an ODE flow through $t = 0$ to $t = 1$ using numerical ODE solver using velocity operator v_θ along this generation process and can generate diverse airfoils. As shown in (c), A single FuncGenFoil model can generate airfoils at arbitrary resolutions, from low to high, while guaranteeing identical outputs when sampling from the same latent function—an inherent property of the model’s architecture.

Then we feed u_t into v_θ and train v_θ by matching the velocity operator:

$$\mathcal{L}_{\text{FM}} = E_{t \sim [0,1], u_0, u_1} [\|v_t - v_\theta(u_t, c, t)\|^2], \quad (3)$$

where v_t is the ground-truth velocity:

$$v_t = u_1 - u_0. \quad (4)$$

Detailed algorithm for training velocity operator is shown in Appendix B Algorithm 2.

Inference. Given a trained velocity operator v_θ , the inference process, *i.e.*, airfoil generation process, is equal to deriving airfoil geometry at time $t = 1$, denoted as u_1 , based on a latent coding u_0 sampled from the stochastic process \mathcal{P} . \mathcal{P} is assumed as a Gaussian Process $\mathcal{GP}(0, K)$, where K is a covariance kernel function. Therefore, u_1 could be derived by solving the ODE in Equation 1 numerically (e.g., using the Euler method) as follows:

$$u_1 = u_0 + \int_{t=0}^{t=1} v_\theta(u_t, c, t) dt. \quad (5)$$

The generation process is shown in Fig. 3 while the detailed algorithm is shown in Appendix B Algorithm 3.

3.2 Airfoil Editing

The airfoil editing task enables the user to modify parts of the geometry of a given airfoil, effectively generating a new airfoil geometry while preserving the user-edited sections, denoted as u_1^δ . We achieve this by an optimization method that maximum a posteriori (MAP) estimation, $\max p(u_1' | u_1^\delta)$ where $p(u_1' | u_1^\delta)$ is a probabilistic model that constrains the optimized airfoil u_1' fulfilling the editing requirements and following the generation prior.

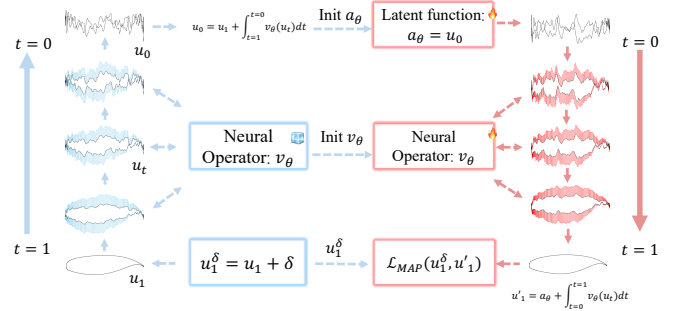


Figure 4: Airfoil editing by **FuncGenFoil**. Given a original airfoil u_1 , an editing requirement δ and target airfoil u_1^δ . We first infer its latent function u_0 reversely, and make it learnable as a_θ . Then we sample a new airfoil u_1' , and conduct a regression in function space via maximum a posteriori estimation $\mathcal{L}_{\text{MAP}}(u_1^\delta, u_1')$. After a few iterations of fine-tuning, we can generate edited airfoil u_1^δ with high accuracy.

To achieve the constraint probability model, we disentangled it with Bayes’ Rule:

$$\begin{aligned} \max_{u_1'} p(u_1' | u_1^\delta) &= \frac{p(u_1^\delta | u_1') \cdot p(u_1')}{p(u_1^\delta)} \\ \Rightarrow \max_{u_1'} \log p(u_1^\delta | u_1') + \log p(u_1') - \log p(u_1^\delta), \end{aligned} \quad (6)$$

where $p(u_1^\delta | u_1')$ is a Gaussian measure, so its log term becomes a Mean Square Error (MSE) between u_1^δ and u_1' , constraining the user edited parts in u_1' keeping consistent with u_1^δ . $p(u_1')$ is the prior supported by the trained generative model so its log value is derived by Hutchinson trace estimator [Hutchinson, 1990; Grathwohl *et al.*, 2019] effectively. $p(u_1^\delta)$ is the marginal likelihood, which does not depend on

Algorithm 1 Airfoil Editing.

Input: pretrained neural operator v_θ , original airfoil function u_1 (optional) or latent function u_0 (optional), editing requirement δ , editing resolution d , sampling time steps T and steps length dt .

Parameter: gaussian process $\mathcal{GP}(0, K)$ for sampling u_0 , noise level σ .

Output: new airfoil $\{y_i\}$ at resolution d .

- 1: Inversely sample original airfoil function $\{u_{1,i}\}$ through v_θ and get its latent function $\{u_{0,i}\}$.
 - 2: Set $\{a_{\theta,i}\} = \{u_{0,i}\}$.
 - 3: **while** finetuning... **do**
 - 4: Sample $\{u'_{1,i}\}$ through v_θ from $\{a_{\theta,i}\}$.
 - 5: Compute \mathcal{L}_{MAP} .
 - 6: Compute gradient and update θ .
 - 7: **end while**
 - 8: Sample $\{u'_{1,i}\}$ through v_θ from $\{a_{\theta,i}\}$.
 - 9: **return** $\{y_i\} = \{u'_{1,i}\}$
-

u'_1 . The final optimization target could be written as:

$$\max_{u'_1} \frac{1}{2\sigma^2} \sum_{i \in \Delta} (u_1^{\delta,i} - u'^{i})^2 + \log p(u'_1), \quad (7)$$

where σ is noise, Δ denotes point indices in edited part u_1^δ .

For more realistic generation results, the optimization does not directly adjust u_1 ; instead, we optimize u'_1 indirectly by fine-tuning the entire generative model for a few iterations. The fine-tuning process is illustrated in Fig. 4, while its details are provided in Alg. 1 in the main text. Specifically, we first initialize u'_1 as a resample data of u_1 , by extracting its latent code, denoted as α_θ , via the inverse of our generative model and re-generating u'_1 from this code. Then we treat Equation 7 as the loss function to train θ of the velocity operator and α_θ simultaneously. After the model training, the new u'_1 is the new edited generation results.

4 Experiments

4.1 Experiment Settings

Tasks. We evaluate two tasks in the airfoil inverse design problem: *conditional airfoil generation* and *freestyle airfoil editing*. In the conditional generation task, the model is given a set of 11 geometric parameters that describe the airfoil geometry. Detailed parameter definitions are provided in the Supplementary Materials. The model must generate airfoils that satisfy these geometric constraints. In the freestyle editing task, the model takes an original airfoil and a target modification, such as adjusting the position of a specific point on the airfoil. *The selected point can be any location on the airfoil surface.* The model must generate an airfoil that reflects the specified modification.

Metrics. We adopt the metrics introduced in AFBench [Liu *et al.*, 2024] to evaluate the generated airfoils:

Label Error measures the difference between the physical parameters of the generated or edited airfoil and the intended

target parameters, calculated as $\sigma_i = |\hat{p}_i - p_i|$, where σ_i is the label error for the i -th parameter, \hat{p}_i is the i -th geometric parameter from the generated airfoil, and p_i is the corresponding target parameter. Smaller values indicate better alignment with the target parameters.

Diversity quantifies the variety of generated airfoils, calculated as $D = \frac{1}{n} \sum_{i=1}^n \log \det(L_{S_i})$, where n is the number of samples, and L_{S_i} is the similarity matrix of the i -th subset, computed based on Euclidean distances between airfoils in the subset. Higher values indicate greater diversity among generated airfoils.

Smoothness measures the geometric smoothness of the generated airfoils, calculated as:

$$M = \sum_{i=1}^N \text{Distance}(P_n, P_{n-1}P_{n+1}), \quad (8)$$

where P_n is the n -th point, and $P_{n-1}P_{n+1}$ is the line segment between adjacent points. The function $\text{Distance}(P_n, P_{n-1}P_{n+1})$ computes the perpendicular distance from P_n to this line segment. Smaller values indicate better geometric quality.

Datasets. To benchmark our method, we conduct experiments on three datasets: UIUC [Selig, 1996], Supercritical Airfoil (Super), and AF-200K. UIUC contains 1,600 designed airfoil geometries. Super focuses on supercritical airfoils and includes approximately 20,000 airfoil samples. AF-200K consists of 200,000 highly diversified airfoil samples.

Baselines. We include the baseline models proposed in AFBench [Liu *et al.*, 2024], specifically the conditional VAE (CVAE), conditional GAN (CGAN), the modified VAE with PARSEC parameters and control keypoints (PK-VAE), along with PK-GAN, PKVAE-GAN, the U-Net-based PK-DIFF, and the transformer-based PK-DIT.

Implementation Details. On the AF-200K dataset, we trained for 2 million iterations with a batch size of 2,048 using 8 NVIDIA 4090 GPUs. On the Supercritical Airfoil dataset, we trained for 1 million iterations with a batch size of 256 on a single NVIDIA 4090 GPU. We use the Matérn kernel function as the kernel for the Gaussian process at time $t = 0$. Other training hyperparameters are detailed in the Supplementary Materials.

4.2 Main Results

Conditional Airfoil Generation.

As shown in Table 1, FuncGenFoil significantly outperforms the strongest baseline method (PK-DIT) across all metrics. For *label error*, FuncGenFoil achieves a reduction in average error by **88.5%** on UIUC, **99%** on Super, and **74.4%** on AF-200K. This substantial decrease in label error underscores the effectiveness of our approach in generating airfoils that more precisely adhere to target geometric parameters. In terms of *diversity*, FuncGenFoil demonstrates notable improvements, surpassing the best baseline methods by **75.4**, **14.6**, and **21.6** on UIUC, Super, and AF-200K, respectively. This highlights the model’s superior capability in capturing and generating a broader spectrum of valid airfoil designs. Additionally, our generated airfoils exhibit enhanced surface *smoothness*, as evidenced by reductions of **0.99** and **4.86** in

Table 1: Quantitative comparison between FuncGenFoil and baseline methods across different datasets for conditional generation task. Label error, diversity, and smoothness of the generated airfoils are reported.

Method	Dataset	Label Error \downarrow (10^{-3})												$\mathcal{D} \uparrow$	$\mathcal{M} \downarrow$ (10^{-2})
		σ_1	σ_2	σ_3	σ_4	σ_5	σ_6	σ_7	σ_8	σ_9	σ_{10}	σ_{11}	$\bar{\sigma}$		
CVAE	AF-200K	72.9	52.5	35.2	15900	99	95	29000	19.1	15.3	46	104	4131	-155.4	7.09
CGAN	AF-200K	107	85.0	54.4	23200	143	137	59600	25.3	22.3	53	129	7596	-120.5	7.31
PK-VAE	AF-200K	63.0	47.9	31.3	8620	66	64	17100	13.5	9.3	33	78	2375	-150.1	5.93
PK-GAN	AF-200K	81.8	63.0	47.0	21030	120	117	32470	22.5	19.6	50	122	4923	-112.3	3.98
PKVAE-GAN	AF-200K	56.8	31.7	31.0	5650	46	43	12000	9.1	5.1	28	63	1633	-129.6	2.89
PK-DIT	AF-200K	11.2	32.3	15.4	1050	13	11.5	9790	0.5	0.5	23	24	997	-93.2	1.04
FuncGenFoil	AF-200K	1.84	17.4	0.56	721	47.7	0.98	1676	0.45	0.65	160	174	255	-71.6	1.41
PK-DIT	UIUC	63.8	51.4	33.6	11830	87	84.9	25700	16.9	11.9	36	98	3456	-141.7	6.03
FuncGenFoil	UIUC	14.2	12.7	0.86	434.9	90.7	3.7	3559	0.55	0.69	129.9	135.2	398.4	-66.3	1.17
PK-DIT	Super	52.0	35.0	24.0	3010	29	33.2	10500	8.3	2.6	27	33	1250	-123.4	1.97
FuncGenFoil	Super	0.73	1.9	0.09	53.2	1.07	0.07	56.4	0.06	0.06	10.5	13.6	12.5	-108.8	0.98

Table 2: Quantitative evaluation of the airfoil editing task across different edit scales. The mean squared error (MSE) between the generated and target airfoils as well as the smoothness of the generated airfoils are reported.

Dataset	Edit Scale	MSE \downarrow (10^{-7})	$\mathcal{M} \downarrow$ (10^{-2})
Super	0.0001	2.41	1.16
	0.0002	2.45	1.15
	0.0004	2.75	1.15

smoothness values (10^{-2}) on the UIUC and Super datasets, respectively. This improvement is particularly crucial for aerodynamic performance, as smoother airfoil surfaces contribute to reduced drag and improved flow characteristics.

Freestyle Airfoil Editing. Table 2 shows the average performance across 300 editing cases using FuncGenFoil. In each case, the model adjusts 2 to 4 randomly selected positions on the wing surface to target locations over 10 fine-tuning steps, with edit scales ranging from 1×10^{-4} to 4×10^{-4} . The results demonstrate that FuncGenFoil can perform accurate airfoil editing with minimal errors (less than 2.75×10^{-7} MSE) and high surface smoothness (less than 1.16×10^{-2} smoothness value) with just a few fine-tuning steps. Fig. 5 illustrates the editing requirements and generated airfoils during the fine-tuning stage. It shows that our model faithfully completes the freestyle editing task by generating reasonable airfoils according to user-specified editing requirements.

Any-Resolution Airfoil Generation. One of the key advantages of FuncGenFoil is its ability to generate airfoils at any resolution while maintaining high generation quality. This is achieved by representing airfoils as functions and learning resolution-independent function transformations, enabling flexible and consistent airfoil generation across different scales. To evaluate high-resolution generation, we use the model trained on the Supercritical Airfoil dataset at a resolution of 257 and sample new airfoils at resolutions of 513 and 1025. We then assess these higher-resolution airfoils using the same metrics as in the conditional

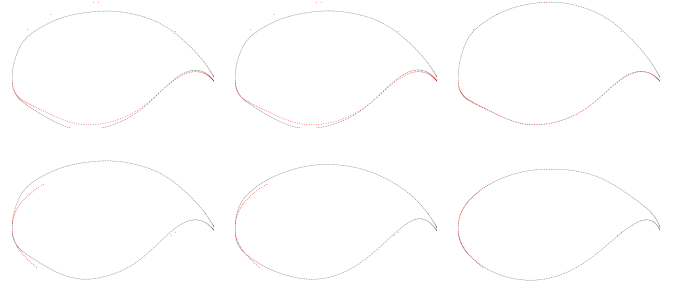


Figure 5: Examples of two FuncGenFoil instances performing airfoil editing over 100 training iterations. The red section represents the editing requirement, while the black airfoil shows the generated samples at each training stage. The results demonstrate that the generated airfoil quickly adapts to the editing requirements within a few iterations, achieving a natural and smooth function regression.

generation task. The results are presented in Table 3. We observe consistent generation quality at $2\times$ and even $4\times$ the training resolution, with a maximum increase of 9.1×10^{-3} in average label error, a decrease of **16.1** in diversity, and an increase of 0.67×10^{-2} in smoothness value.

Aerodynamic Simulation. To further assess the physical properties of the generated airfoils and validate the effectiveness of our method, we analyze their aerodynamic performance using the NASA Common Research Model (CRM) ² and perform Reynolds-Averaged Navier-Stokes (RANS) computational fluid dynamics (CFD) simulations on the generated samples. The CRM dataset contains 135,000 CRM wing geometries along with their corresponding aerodynamic performance, computed using the RANS CFD solver ADflow [Mader *et al.*, 2020]. We pretrain the FuncGenFoil model on all 135,000 CRM wing geometries and generate 500 new CRM wing geometries for RANS CFD evaluation. We analyze the lift-to-drag ratio (L/D) of these newly generated geometries and compare them with the orig-

²<https://commonresearchmodel.larc.nasa.gov/>

Table 3: Quantitative evaluation of our model (training resolution=257) across different sampling resolutions for conditional generation task.

Dataset	Resolution	Label Error \downarrow (10^{-3})											$\mathcal{D} \uparrow$	$\mathcal{M} \downarrow$ (10^{-2})	
		σ_1	σ_2	σ_3	σ_4	σ_5	σ_6	σ_7	σ_8	σ_9	σ_{10}	σ_{11}			$\bar{\sigma}$
Super	257	0.73	1.9	0.09	53.2	1.07	0.07	56.4	0.06	0.06	10.5	13.6	12.5	-108.8	0.98
	513	0.74	2.59	0.13	55.1	1.54	0.09	57.7	0.07	0.08	41.1	40.0	18.1	-100.5	0.49
	1025	0.75	3.18	0.17	56.5	2.03	0.12	59.2	0.07	0.09	60.8	55.0	21.6	-92.9	0.31

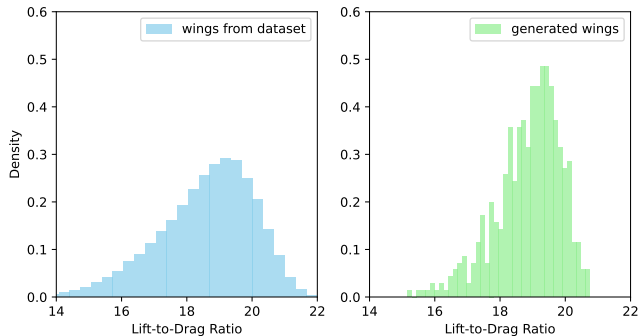


Figure 6: Comparison of the lift-to-drag ratio histograms for CRM wings in the original dataset and the samples generated by our FuncGenFoil model.

inal dataset, as shown in Fig. 6. Our results indicate that the L/D distribution of the generated samples closely aligns with that of the original dataset, with the highest density occurring around $L/D = 19$, demonstrating the model’s ability to learn and generate physically plausible wing geometries. Additionally, we visualize the coefficient of pressure contours for selected CFD cases in Fig. 7. These visualizations confirm that FuncGenFoil can generate airfoils with diverse aerodynamic performance characteristics.

4.3 Ablation Study

We first ablate the use of the Matérn kernel K with different parameters as the kernel function for the sampled Gaussian process. As shown in Table 4, we compare the cases of Matérn kernel $\nu = 1.5$, $l = 0.01$, and Matérn kernel $\nu = 2.5$, $l = 0.03$, where the latter is smoother due to the combined effect of both parameters. Notably, the limits of $l = 0$ and $\nu \rightarrow \infty$ correspond to pure white noise and the RBF kernel, respectively. To further highlight the importance of kernel function selection, we also test two models of different sizes (by setting different FNO modes). From Table 4, we observe that a smoother kernel improves both the smoothness and accuracy of the generated airfoils. Additionally, the comparison highlights that, under our setup, selecting a smoother kernel leads to a more substantial performance improvement than increasing the model size. This underscores the benefit of modeling the function object in the airfoil generation task rather than modeling discrete points.

In Table 5, we compare the MSE of constraint condition calculations in the airfoil editing task using two initialization schemes: (1) using the latent variables obtained through ODE inversion of the original airfoil as the prior, and (2) using a zero prior $u_0 = 0$ without ODE inversion. Both schemes

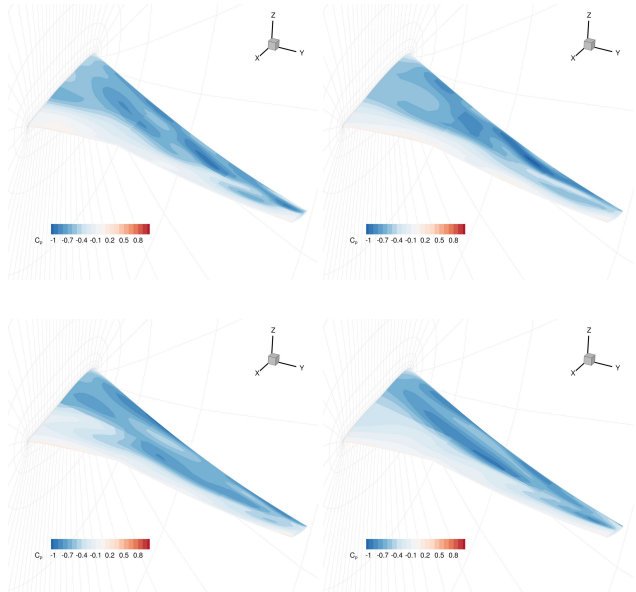


Figure 7: Visualization of the pressure coefficient for the generated CRM wings, obtained through aerodynamic simulation.

Table 4: Ablation study on the impact of different kernels and model sizes for the conditional airfoil generation task.

Matérn ν	Matérn l	FNO modes	$\bar{\sigma} \downarrow$	$\mathcal{M} \downarrow$
1.5	0.01	32	0.108	0.0119
2.5	0.03	32	0.013	0.0098
1.5	0.01	48	0.039	0.0101
2.5	0.03	48	0.013	0.0098

are fine-tuned with the same number of iterations. As shown, the ODE inversion-based prior significantly reduces the MSE compared to the zero prior, with a maximum reduction of **84.85**. This underscores the importance of incorporating original airfoil information during the initialization process.

5 Conclusion

In this work, we tackle the critical challenge of generating high-fidelity airfoil geometries that effectively balance expressiveness, smoothness, and resolution flexibility. We introduce **FuncGenFoil**, a function-space generative model leveraging neural operators and flow matching, which represents airfoils as continuous, smooth geometries without resolution constraints while preserving the expressiveness of data-driven methods. Comprehensive experimental results show

Table 5: Ablation study on the effect of different latent variable initialization methods for the airfoil editing task.

Edit scale	MSE↓(10 ⁻⁷)	
	w/ ODE inversion	w/o ODE inversion
0.0001	2.42 (↓83.88)	86.3
0.0002	2.46 (↓84.14)	86.6
0.0004	2.75 (↓84.85)	87.6

that FuncGenFoil outperforms state-of-the-art techniques in terms of label error, diversity, and smoothness, highlighting its potential for high-fidelity airfoil design. Furthermore, the generated wing geometries have been validated through aerodynamic simulations. This work paves the way for more efficient, scalable, and versatile airfoil generation, with significant applications in aerodynamic shape optimization for aircraft manufacturing.

References

- [Anandkumar *et al.*, 2019] Anima Anandkumar, Kamyar Azizzadenesheli, Kaushik Bhattacharya, Nikola Kovachki, Zongyi Li, Burigede Liu, and Andrew Stuart. Neural operator: Graph kernel network for partial differential equations. In *ICLR 2020 Workshop on Integration of Deep Neural Models and Differential Equations*, 2019.
- [Azizzadenesheli *et al.*, 2024] Kamyar Azizzadenesheli, Nikola Kovachki, Zongyi Li, Miguel Liu-Schiaffini, Jean Kossaifi, and Anima Anandkumar. Neural operators for accelerating scientific simulations and design. April 2024.
- [Berkooz *et al.*, 1993] Gal Berkooz, Philip Holmes, and John L. Lumley. The proper orthogonal decomposition in the analysis of turbulent flows. *Annual Review of Fluid Mechanics*, 1993.
- [Brüls *et al.*, 2007] Olivier Brüls, Pierre Duysinx, and Jean-Claude Golinval. The global modal parameterization for non-linear model-order reduction in flexible multibody dynamics. *International journal for numerical methods in engineering*, 2007.
- [Cao, 2021] Shuhao Cao. Choose a transformer: Fourier or galerkin. *NIPS*, 34:24924–24940, 2021.
- [Chen and Fuge, 2021] Wei Chen and Mark Fuge. Béziergan: Automatic generation of smooth curves from interpretable low-dimensional parameters, 2021.
- [Cummings *et al.*, 2015] Russell M Cummings, William H Mason, Scott A Morton, and David R McDaniel. *Applied computational aerodynamics: A modern engineering approach*, volume 53. Cambridge University Press, 2015.
- [Dannenhoffer, 2024] III Dannenhoffer, John F. An overview of the engineering sketch pad. In *AIAA SciTech 2024 Forum*, Orlando, FL, January 2024.
- [Dupont *et al.*, 2022a] Emilien Dupont, Hyunjik Kim, S. M. Ali Eslami, Danilo Jimenez Rezende, and Dan Rosenbaum. From data to functa: Your data point is a function and you can treat it like one. In Kamalika Chaudhuri, Stefanie Jegelka, Le Song, Csaba Szepesvari, Gang Niu, and Sivan Sabato, editors, *ICML*, Proceedings of Machine Learning Research. PMLR, 2022.
- [Dupont *et al.*, 2022b] Emilien Dupont, Yee Whye Teh, and Arnaud Doucet. Generative models as distributions of functions. In Gustau Camps-Valls, Francisco J. R. Ruiz, and Isabel Valera, editors, *AISTATS*. PMLR, 2022.
- [Farin, 2002] Gerald E. Farin. *Curves and Surfaces for CAD: A Practical Guide*. Morgan Kaufmann, 2002.
- [Franzese *et al.*, 2024] Giulio Franzese, Giulio Corallo, Simone Rossi, Markus Heinonen, Maurizio Filippone, and Pietro Michiardi. Continuous-time functional diffusion processes. *NeurIPS*, 36, 2024.
- [Garnelo *et al.*, 2018a] Marta Garnelo, Dan Rosenbaum, Christopher Maddison, Tiago Ramalho, David Saxton, Murray Shanahan, Yee Whye Teh, Danilo Rezende, and S. M. Ali Eslami. Conditional neural processes. In Jennifer Dy and Andreas Krause, editors, *ICML*, Proceedings of Machine Learning Research. PMLR, 2018.
- [Garnelo *et al.*, 2018b] Marta Garnelo, Jonathan Schwarz, Dan Rosenbaum, Fabio Viola, Danilo J. Rezende, S. M. Ali Eslami, and Yee Whye Teh. Neural processes, 2018.
- [Gat *et al.*, 2024] Itai Gat, Tal Remez, Neta Shaul, Felix Kreuk, Ricky T. Q. Chen, Gabriel Synnaeve, Yossi Adi, and Yaron Lipman. Discrete flow matching. In *NeurIPS*, 2024.
- [Grathwohl *et al.*, 2019] Will Grathwohl, Ricky T. Q. Chen, Jesse Bettencourt, and David Duvenaud. Scalable reversible generative models with free-form continuous dynamics. In *ICML*, 2019.
- [Hahn, 2010] Andrew S. Hahn. Vehicle sketch pad: A parametric geometry modeler for conceptual aircraft design. In *48th AIAA Aerospace Sciences Meeting Including the New Horizons Forum and Aerospace Exposition*, 2010.
- [Ho *et al.*, 2020a] Jonathan Ho, Ajay Jain, and Pieter Abbeel. Denoising diffusion probabilistic models. In H Larochelle, M Ranzato, R Hadsell, M F Balcan, and H Lin, editors, *NIPS*, volume 33, pages 6840–6851. Curran Associates, Inc., 2020.
- [Ho *et al.*, 2020b] Jonathan Ho, Ajay Jain, and Pieter Abbeel. Denoising diffusion probabilistic models. *NIPS*, 33:6840–6851, 2020.
- [Ho *et al.*, 2022] Jonathan Ho, Tim Salimans, Alexey Gritsenko, William Chan, Mohammad Norouzi, and David J Fleet. Video diffusion models. In S. Koyejo, S. Mohamed, A. Agarwal, D. Belgrave, K. Cho, and A. Oh, editors, *NeurIPS*, volume 35, pages 8633–8646. Curran Associates, Inc., 2022.
- [Hutchinson, 1990] M.F. Hutchinson. A stochastic estimator of the trace of the influence matrix for laplacian smoothing splines. *Communications in Statistics - Simulation and Computation*, 1990.
- [Kerrigan *et al.*, 2023] Gavin Kerrigan, Justin Ley, and Padhraic Smyth. Diffusion generative models in infinite

- dimensions. In Francisco Ruiz, Jennifer Dy, and Jan-Willem van de Meent, editors, *AISTATS*, volume 206 of *Proceedings of Machine Learning Research*, pages 9538–9563. PMLR, 25–27 Apr 2023.
- [Kerrigan *et al.*, 2024] Gavin Kerrigan, Giosue Migliorini, and Padhraic Smyth. Functional flow matching. In *Proceedings of The 27th International Conference on Artificial Intelligence and Statistics*, 2024.
- [Kingma, 2013] Diederik P Kingma. Auto-encoding variational bayes. *arXiv preprint arXiv:1312.6114*, 2013.
- [Kovachki *et al.*, 2023] Nikola Kovachki, Zongyi Li, Burigede Liu, Kamyar Azizzadenesheli, Kaushik Bhattacharya, Andrew Stuart, and Anima Anandkumar. Neural operator: learning maps between function spaces with applications to pdes. *J. Mach. Learn. Res.*, 24(1), January 2023.
- [Kulfan, 2008] B. M. Kulfan. Universal parametric geometry representation method. *Journal of Aircraft*, 2008.
- [Li and Zhang, 2021] Jichao Li and Mengqi Zhang. Adjoint-free aerodynamic shape optimization of the common research model wing. *AIAA Journal*, 2021.
- [Li *et al.*, 2021] Zongyi Li, Nikola Borislavov Kovachki, Kamyar Azizzadenesheli, Burigede liu, Kaushik Bhattacharya, Andrew Stuart, and Anima Anandkumar. Fourier neural operator for parametric partial differential equations. In *ICLR*, 2021.
- [Li *et al.*, 2022] Jichao Li, Xiaosong Du, and Joaquim RRA Martins. Machine learning in aerodynamic shape optimization. *Progress in Aerospace Sciences*, 134:100849, 2022.
- [Lim *et al.*, 2023] Jen Ning Lim, Sebastian Vollmer, Lorenz Wolf, and Andrew Duncan. Energy-based models for functional data using path measure tilting. In *AISTATS*, 2023.
- [Lim *et al.*, 2025] Jae Hyun Lim, Nikola B. Kovachki, Ricardo Baptista, Christopher Beckham, Kamyar Azizzadenesheli, Jean Kossaiji, Vikram Voleti, Jiaming Song, Karsten Kreis, Jan Kautz, Christopher Pal, Arash Vahdat, and Anima Anandkumar. Score-based diffusion models in function space, 2025.
- [Lipman *et al.*, 2022] Yaron Lipman, Ricky TQ Chen, Heli Ben-Hamu, Maximilian Nickel, and Matt Le. Flow matching for generative modeling. *arXiv preprint arXiv:2210.02747*, 2022.
- [Lipman *et al.*, 2023] Yaron Lipman, Ricky T. Q. Chen, Heli Ben-Hamu, Maximilian Nickel, and Matthew Le. Flow matching for generative modeling. In *ICML*, 2023.
- [Liu *et al.*, 2024] Jian Liu, Jianyu Wu, Hairun Xie, Guoqing Zhang, Jing Wang, Wei Liu, Wanli Ouyang, Junjun Jiang, Xianming Liu, Shixiang Tang, et al. Afbench: A large-scale benchmark for airfoil design. In *NeurIPS 2024 Dataset and Benchmark Track*, 2024.
- [Mader *et al.*, 2020] Charles A. Mader, Gaetan K. W. Kenway, Anil Yildirim, and Joaquim R. R. A. Martins. ADflow—an open-source computational fluid dynamics solver for aerodynamic and multidisciplinary optimization. *Journal of Aerospace Information Systems*, 2020.
- [Mildenhall *et al.*, 2021] Ben Mildenhall, Pratul P Srinivasan, Matthew Tancik, Jonathan T Barron, Ravi Ramamoorthi, and Ren Ng. Nerf: Representing scenes as neural radiance fields for view synthesis. *Communications of the ACM*, 65(1):99–106, 2021.
- [Mirza, 2014] Mehdi Mirza. Conditional generative adversarial nets. *arXiv preprint arXiv:1411.1784*, 2014.
- [Mortenson, 1999] Michael E. Mortenson. *Mathematics for Computer Graphics Applications*. 1999.
- [Pidstrigach *et al.*, 2023] Jakiw Pidstrigach, Youssef Marzouk, Sebastian Reich, and Sven Wang. Infinite-dimensional diffusion models, 2023.
- [Polyak *et al.*, 2024] Adam Polyak, Amit Zohar, and Andrew Brown et al. Movie gen: A cast of media foundation models, 2024.
- [Rahimi and Recht, 2007] Ali Rahimi and Benjamin Recht. Random features for large-scale kernel machines. *NIPS*, 20, 2007.
- [Rahman *et al.*, 2022] Md Ashiqur Rahman, Manuel A Florez, Anima Anandkumar, Zachary E Ross, and Kamyar Azizzadenesheli. Generative adversarial neural operators. *TMLR*, 2022.
- [Rasmussen, 2003] Carl Edward Rasmussen. Gaussian processes in machine learning. In *Summer school on machine learning*. Springer, 2003.
- [Rombach *et al.*, 2022] Robin Rombach, Andreas Blattmann, Dominik Lorenz, Patrick Esser, and Björn Ommer. High-resolution image synthesis with latent diffusion models. In *CVPR*, pages 10684–10695, 2022.
- [Schoenberg, 1964] I. J. Schoenberg. Spline functions and the problem of graduation. *Proceedings of the National Academy of Sciences of the United States of America*, 52(4):947–950, October 1964.
- [Sekar *et al.*, 2019] Vinothkumar Sekar, Mengqi Zhang, Chang Shu, and Boo Cheong Khoo. Inverse design of airfoil using a deep convolutional neural network. *AIAA Journal*, 2019.
- [Selig, 1996] Michael S Selig. Uic airfoil database. 1996.
- [Sharma *et al.*, 2021] Prashant Sharma, Bhupendra Gupta, Mukesh Pandey, Arun Kumar Sharma, and Raji Nareliya Mishra. Recent advancements in optimization methods for wind turbine airfoil design: A review. *Materials Today: Proceedings*, 2021.
- [Shi *et al.*, 2024] Yaozhong Shi, Angela F Gao, Zachary E Ross, and Kamyar Azizzadenesheli. Universal functional regression with neural operator flows. In *NeurIPS 2024 Workshop on Bayesian Decision-making and Uncertainty*, 2024.
- [Shi *et al.*, 2025] Yaozhong Shi, Zachary E. Ross, Domniki Asimaki, and Kamyar Azizzadenesheli. Stochastic process learning via operator flow matching, 2025.

- [Sitzmann *et al.*, 2020] Vincent Sitzmann, Julien Martel, Alexander Bergman, David Lindell, and Gordon Wetzstein. Implicit neural representations with periodic activation functions. *Advances in neural information processing systems*, 33:7462–7473, 2020.
- [Song *et al.*, 2021] Yang Song, Jascha Sohl-Dickstein, Diederik P Kingma, Abhishek Kumar, Stefano Ermon, and Ben Poole. Score-based generative modeling through stochastic differential equations. In *ICLR*, 2021.
- [Tong *et al.*, 2024] Alexander Tong, Kilian FATRAS, Nikolay Malkin, Guillaume Huguet, Yanlei Zhang, Jarrid Rector-Brooks, Guy Wolf, and Yoshua Bengio. Improving and generalizing flow-based generative models with minibatch optimal transport. *TMLR*, 2024. Expert Certification.
- [Wei *et al.*, 2023] Zhen Wei, Benoît Guillard, Pascal Fua, Vincent Chapin, and Michaël Bauerheim. Latent representation of computational fluid dynamics meshes and application to airfoil aerodynamics. *AIAA Journal*, 2023.
- [Wei *et al.*, 2024a] Zhen Wei, Edouard R. Dufour, Colin Pelletier, Pascal Fua, and Michaël Bauerheim. Diffairfoil: An efficient novel airfoil sampler based on latent space diffusion model for aerodynamic shape optimization. In *AIAA AVIATION FORUM AND ASCEND*, 2024.
- [Wei *et al.*, 2024b] Zhen Wei, Aobo Yang, Jichao Li, Michaël Bauerheim, Rhea P. Liem, and Pascal Fua. Deepgeo: Deep geometric mapping for automated and effective parameterization in aerodynamic shape optimization. In *AIAA AVIATION FORUM AND ASCEND*, 2024.
- [Xie *et al.*, 2024] Hairun Xie, Jing Wang, and Miao Zhang. Parametric generative schemes with geometric constraints for encoding and synthesizing airfoils. *Engineering Applications of Artificial Intelligence*, 2024.
- [Yang *et al.*, 2024] Aobo Yang, Jinouwen Zhang, Jichao Li, and Rhea Liem. Data-driven aerodynamic shape optimization and multi-fidelity design exploration using conditional diffusion-based geometry sampling method. In *ICAS*, 2024.

A Airfoil Geometry Parameters

We adopted the same conditions and symbols as those in AFBench. The parameters below, including the leading-edge radius, the curvature at the maximum thickness of the upper and lower surfaces, and the trailing-edge angle of the airfoil, were obtained through fitting. Note that our implementation of the angle calculation differs slightly from that of AFBench, as we found that the original fitting method was not invariant when the sampling precision increased.

B Algorithm Details

The algorithm for training airfoil generative models is shown in Algorithm 2, and inference using a trained model is shown in Algorithm 3. In the actual implementation, we utilized Optimal Transport techniques and employed the Matérn kernel as the kernel function for the Gaussian process in the latent space of the generative model.

Table 6: Geometric parameters of the airfoils used in conditional generation tasks

Index	Symbol	Meaning
1	R_{le}	the leading edge radius
2	X_{up}	upper crest position x
3	Y_{up}	upper crest position y
4	Z_{xxup}	upper crest curvature
5	X_{lo}	lower crest position x
6	Y_{lo}	lower crest position y
7	Z_{xxlo}	lower crest curvature
8	Y_{te}	trailing edge position
9	ΔY_{te}	trailing thickness
10	α_{te}	trailing edge angle up
11	β_{te}	trailing edge angle down

Algorithm 2 Generative Model Training.

Input: data resolution d , data u_1 , design condition variables c (optional).

Parameter: gaussian process $\mathcal{GP}(\mathbf{0}, K)$ for sampling u_0 .

Output: velocity operator v_θ .

- 1: **while** training... **do**
- 2: sample $t \sim [0, 1]$, $u_0 \sim \mathcal{GP}(\mathbf{0}, K)$ at resolution d and get $\{u_{0,i}\}$.
- 3: Compute v_t at resolution d and get $\{v_{t,i}\}$.
- 4: Compute u_t at resolution d and get $\{u_{t,i}\}$.
- 5: Compute $v_\theta(u_t, c, t)$ at resolution d and get $\{v_{\theta,i}\}$.
- 6: Minimize $\|\{v_{\theta,i}\} - \{v_{t,i}\}\|^2$.
- 7: Compute gradient and update θ .
- 8: **end while**
- 9: **return** v_θ .

C Training Details

In most of the experiments, we followed the hyperparameters listed in the table below to train the models, including both the pre-training and fine-tuning stages. On the AF-200K dataset, we increased the maximum number of iterations to 2,000,000 and the batch size to 2048. For the number of time steps used to solve the ODE, we tested reconstruction metrics on the super dataset with 10, 100, and 1000 steps, and ultimately chose 100 steps as the default setting for all other experiments, except for the fine-tuning stage, where we used 10 steps for training efficiency.

Algorithm 3 Inference Process (Airfoil Generation)

Input: sampling resolution d , sampling time steps T and steps length dt , latent function u_0 (optional), design condition variables c (optional).

Parameter: gaussian process $\mathcal{GP}(\mathbf{0}, K)$ for sampling u_0 .

Output: airfoil $\{y_i\}$ at resolution d .

- 1: Let $t = \mathbf{0}$, $u_0 \sim \mathcal{GP}(\mathbf{0}, K)$ at resolution d and get $\{u_{0,i}\}$.
 - 2: **while** $t \leq 1$ **do**
 - 3: Compute $v_\theta(u_t, c, t)$ at resolution d and get $\{v_{\theta,i}\}$.
 - 4: Compute $\{u_{t+dt,i}\} = \{u_{t,i}\} + \{v_{\theta,i}dt\}$.
 - 5: $t = t + dt$.
 - 6: **end while**
 - 7: **return** $\{y_i\} = \{u_{1,i}\}$
-

Table 7: Training hyperparameters and model parameters in conditional airfoils generation tasks

Training hyperparameters	Value
max learning rate	5e-6
batch size	512
optimizer used in pre-training and finetuning	Adam
train max iterations	1,000,000
ODE Solver time steps	100
Model parameters	Value
Fourier neural operator layers	8
Fourier neural operator modes	48
Fourier neural operator hidden channels	256
Matérn kernel ν	2.5
Matérn kernel l	0.03